JOURNAL OF GEOPHYSICAL RESEARCH: ATMOSPHERES, VOL. 118, 1–15, doi:10.1029/2012JD018124, 2013

Characteristics of stratosphere-troposphere exchange during the Meiyu season

Jiali Luo,[1] Wenshou Tian,[1] Zhaoxia Pu,[2] Peiqun Zhang,[3] Lin Shang,[1] Min Zhang,[4] and Jun Hu[5]

Received 17 May 2012; revised 31 October 2012; accepted 1 November 2012.

[1] Characteristics of stratosphere-troposphere exchange (STE) during the Meiyu season in the Yangtze-Huaihe valley, China, is investigated using the European Centre for Medium-Range Weather Forecasts interim reanalysis data, National Centers for Environmental Prediction/National Center for Atmospheric Research reanalysis data, Meiyu records from the National Climate Center of China, the data from a trajectory model, and a general circulation model (GCM). Results show increases in potential vorticity and decreases in specific humidity in the upper troposphere and lower stratosphere (UTLS) before Meiyu onset, suggesting a strong downward transport of air masses around the tropopause that can be attributed to frequent tropopause folds over the Meiyu area. The minimum tropopause height occurs 3 days before Meiyu onset and then rises until about 6 days afterward. The downward cross-tropopause mass transport (CTMF) is evidenced before Meiyu onset, which is mainly caused by the sharp meridional gradients in the tropopause pressure over the Meiyu area. After Meiyu onset, the upward cross-tropopause transport intensifies due to enhanced convections. The analysis also suggests the strongest upward transport in the UTLS occurs northeast of the Meiyu region, within the core of the upper tropospheric westerly jet. Results from a trajectory model indicate that the lower stratospheric air intrudes into the troposphere before Meiyu onset. The significant upward movements of the middle tropospheric air are notable after Meiyu onset. As convections are weak and the upper level westerly jet is located far to the Meiyu area in poor Meiyu years, the upward CTMF over the Meiyu region is weaker during the Meiyu season compared with that in rich Meiyu years.

Citation: Luo, J., W. Tian, Z. Pu, P. Zhang, L. Shang, M. Zhang, and J. Hu (2013), Characteristics of stratosphere-troposphere exchange during the Meiyu season, *J. Geophys. Res. Atmos.*, *118*, doi:10.1029/2012JD018124.

1. Introduction

[2] The rate at which air masses are exchanged across the tropopause is one of the key open questions regarding the global budget of various chemical species. Studies in recent years have found convincing evidence that the monsoon has significant impact on stratosphere troposphere exchange (STE) [e.g., *Zachariasse et al*., 2000; *Fu et al*., 2006; *Randel et al*., 2010]. *Gettleman et al*. [2004] pointed out that the Asian monsoon circulation may contribute 75% of the total net upward water vapor flux in the tropics at tropopause level from July to September. *Park et al*. [2004] found from chemical transport model simulations that the air from the monsoon region can be transported into the tropics by the monsoon circulation and be taken into the stratosphere by the upward Brewer-Dobson circulation.

[3] During the Asian summer monsoon season, from the middle to lower reaches of the Yangtze River in China to southwestern Japan, a precipitation zone occurs and lasts for several weeks with major rainband advancing poleward from south (premonsoon, May) to central (June) to north (July) China [*Liang and Wang*, 1998]. This phenomenon, which occurs concurrently with the onset of the summer southwest monsoon over the South China Sea, is called Meiyu in China and Baiu in Japan [*Zhou et al*., 2004]. A great many studies have been carried out to understand Meiyu as a weather phenomenon on the mesoscale and synoptic scale [e.g., *Krishnan and Sugi*, 2001; *Ninomiya and Shibagaki*, 2007; *Wakazuki et al*., 2006; *Ninomiya*, 2000, 2001; *Ninomiya and Murakami*, 1987; *Tao and Chen*, 1987; *Ding*, 1991; *Ninomiya and Akiyama*, 1992; *Kawatani and Takahashi*, 2003; *Yoshikane et al*., 2001; *Moteki et al*.,

[1]Key Laboratory of Semi-Arid Climate Change and College of Atmospheric Sciences, Lanzhou University, Lanzhou, China.
[2]Department of Atmospheric Sciences, University of Utah, Salt Lake City, Utah, USA.
[3]National Climate Center, Beijing, China.
[4]Inner Mongolia Autonomous Region Meteorological Observatory, Hohhot, China.
[5]State Key Laboratory of Numerical Modeling for Atmospheric Sciences and Geophysical Fluid Dynamics, Beijing, China.

Corresponding author: W. Tian, College of Atmospheric Sciences, Lanzhou University, Lanzhou 730000, China. (wstian@lzu.edu.cn)

2169-897X/13/2012JD018124

2006; *Chen et al*., 2003]. Distinct features of Meiyu are found to be strong moisture flux, flux convergence and heavy rainfall over the Meiyu region while the associated Meiyu front is quasi-stationary and can generate long cloud and rainbands. Within this rainband, mesoscale disturbances develop accompanied by the intense convection [e.g., *Ninomiya and Shibagaki*, 2007]. *Sampe and Xie* [2010] pointed that there is a remarkable correspondence between the warm advection and upward motion along the Meiyu-Baiu rainband.

[4] Since Meiyu is characterized with strong flux convergence and frequent occurrences of mesoscale convective systems, one may expect that Meiyu should have a potential impact on the STE over the Meiyu region. *Yasunari and Miwa* [2006] have found that even convective activities over the Tibetan Plateau were closely associated with the mesoscale cloud systems in the Meiyu frontal zone. However, the characteristic and properties of the STE in the Meiyu season over the Meiyu region have not been well understood yet. Although previous studies have shown the importance of the Monsoon circulation in modulating STE, those studies mainly focused on the STE over the Tibetan Plateau or in tropics [e.g., *Randel et al*., 2010; *Gettleman et al*., 2004]. The STE properties over the Meiyu region during the Meiyu season have been rarely addressed in the previous literature.

[5] In this study, the bulk properties of stratosphere-troposphere exchange over the Yangtze-Huaihe valley, China, in the Meiyu season are analyzed using European Centre for Medium-Range Weather Forecasts (ECMWF) interim reanalysis (ERA-Interim) data and historical Meiyu records provided by the National Climate Center of China. Section 2 briefly describes the data and analysis methods. The modulations of Meiyu on water vapor and potential vorticity in the upper troposphere and lower stratosphere (UTLS) are discussed in section 3. The variations of the cross-tropopause mass flux around the Meiyu season are presented in section 4. Section 5 shows results of the trajectory analysis. Section 6 gives summaries and conclusions.

2. Data and Method

[6] Data used in this study are 6-hourly ERA-Interim reanalysis data, 6-hourly National Centers for Environmental Prediction/National Center for Atmospheric Research (NCEP/NCAR) reanalysis data, and annual Meiyu records from the National Climate Center of China. Both data sets span the time period from 1989 to 2008 for a total of 20 years. Annual Meiyu records from National Climate Center of China includes the day Meiyu onsets the day Meiyu stops, the precipitation during the Meiyu season and other records. The Meiyu onset date is determined from the precipitation data at the five selected stations which are sparsely distributed within the Meiyu area together with the position of the subtropical ridge. For a given day, if the daily precipitation at more than 2 stations among these 5 selected stations greater than 0.1 mm and the total precipitation of the 5 stations is greater than 10 mm, this day is referred as a rain day in the Meiyu area. And then, if rain days during a period from the first rain day to subsequent 10 days are great than 5 days and the position of the subtropical ridge is located at the latitude band from 20°N to 25°N, the first rain day is determined as the Meiyu onset date. The Meiyu region is confined to 28°N–34°N,110°E–122°E (Figure 1) according to the definition in *Hu et al*. [2008]. A composite analysis is performed with respect to days before and after Meiyu onset. During the 20 yr study period, 2000 and 2002 are excluded for the composite analysis as there was no Meiyu occurred in these 2 years. The composite fields for the *n*th day before (or after) Meiyu onset are calculated by averaging over 18 years of the *n*th day data. All together 30 days of composites are made with 15 days of composites before Meiyu onset and 15 days of composites after Meiyu onset. The percentage difference ($\Phi_{\bar{d}} \times 100$) of a field Φ is defined as follow except otherwise stated,

$$\Phi_{\bar{d}} = (\Phi_{\bar{a}} - \Phi_{\bar{b}})/\Phi_{\bar{c}} \tag{1}$$

where $\Phi_{\bar{a}}$ and $\Phi_{\bar{b}}$ are the mean Φ averaged over 15 days after Meiyu onset and 15 days before Meiyu onset, respectively.

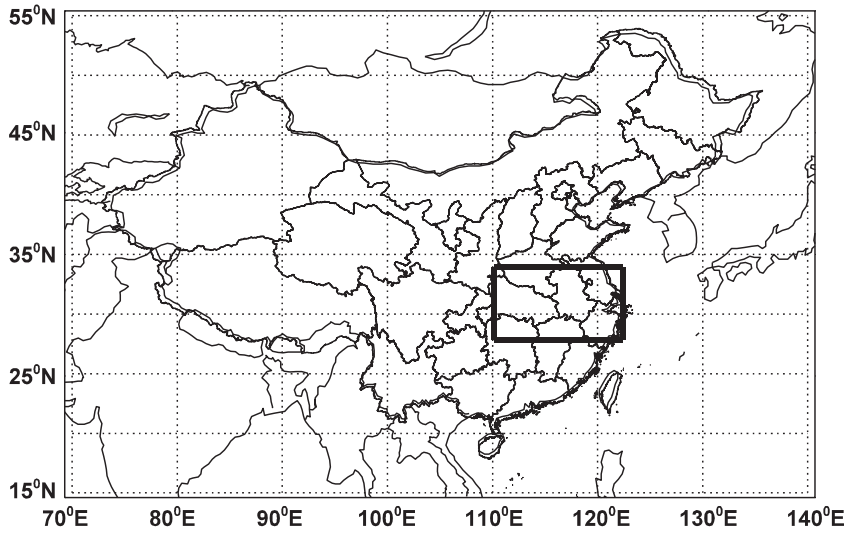

Figure 1. The geographical map of China. The rectangle indicates the Meiyu region.

$\Phi_{\bar{c}}$ is the mean of $\Phi_{\bar{a}}$ and $\Phi_{\bar{b}}$. The absolute differences are defined as 15-day mean fields after Meiyu onset minus corresponding 15-day mean fields before Meiyu onset. As the thermal tropopause has discontinuities in the extratropics, the dynamical tropopause, which is determined by the potential vorticity (PV) of 3.0 pvu (PV units, 1 pvu = 10^{-6} m^2 s^{-1} K kg^{-1}), is used in cross-tropopause mass flux calculations.

[7] A long-term climate model simulation from 1981 to 2010 was also performed to compare the climate feature of the CTMF during the Meiyu season diagnosed from reanalysis data and the model simulation. The model used is the Whole Atmosphere Community Climate Model, version 3 (WACCM3) which has 66 vertical levels from the ground to 4.5×10^{-6} hPa and the model's vertical resolution is 1.1–1.4 km in the UTLS [*Garcia et al*., 2007]. The simulation presented in this paper has been performed at $1.9° \times 2.5°$ resolution with the interactive chemistry switched off. The sea surface temperature (SST) and sea ice fields used in the simulation are monthly mean, time varying observations provided by the Meteorological Office, Hadley Centre for Climate Prediction and Research [*Rayner et al*., 2006].

3. Variations of UTLS PV and Water Vapor

[8] The variations of PV and water vapor in the UTLS region during the Meiyu season are examined first. Figures 2a and 2b show time-height cross sections of composited the potential vorticity (PV) and specific humidity in the UTLS, averaged over the Meiyu area from 15 days before Meiyu onset to 15 days after Meiyu onset. It is apparent that PV reaches their peak values on the third day before Meiyu onset and then drops sharply when Meiyu is onset. In contrast, specific humidity shows an opposite variation with time, i.e., it increases significantly after Meiyu onset. Note that the significant variations of PV and specific humidity before Meiyu onset can be clearly seen from 150 to 100 hPa. As PV increases with height, specific humidity decreases with height, the lower PV but higher water vapor found in the UTLS after Meiyu onset suggests upward transport of air masses in the UTLS over the Meiyu region. Meanwhile, evident increases in PV and a decrease in specific humidity before Meiyu onset imply strong downward transport of air masses in the UTLS. Figures 2c and 2d show the percentage differences in PV and specific humidity fields at 150 hPa before and after Meiyu onset. Hereafter, the differences of these fields before and after Meiyu onset will be referred as anomalies of corresponding fields wherever appropriate. Corresponding to Figures 2a and 2b, a belt of low PV, together with high specific humidity around the Meiyu region is evident in Figures 2c and 2d, although the maximum of specific humidity anomalies and the minimum of PV anomalies are not collocated exactly. The region of minimum PV anomalies is located northeast of the Meiyu region (115°–134°E, 32°–36°N) while the

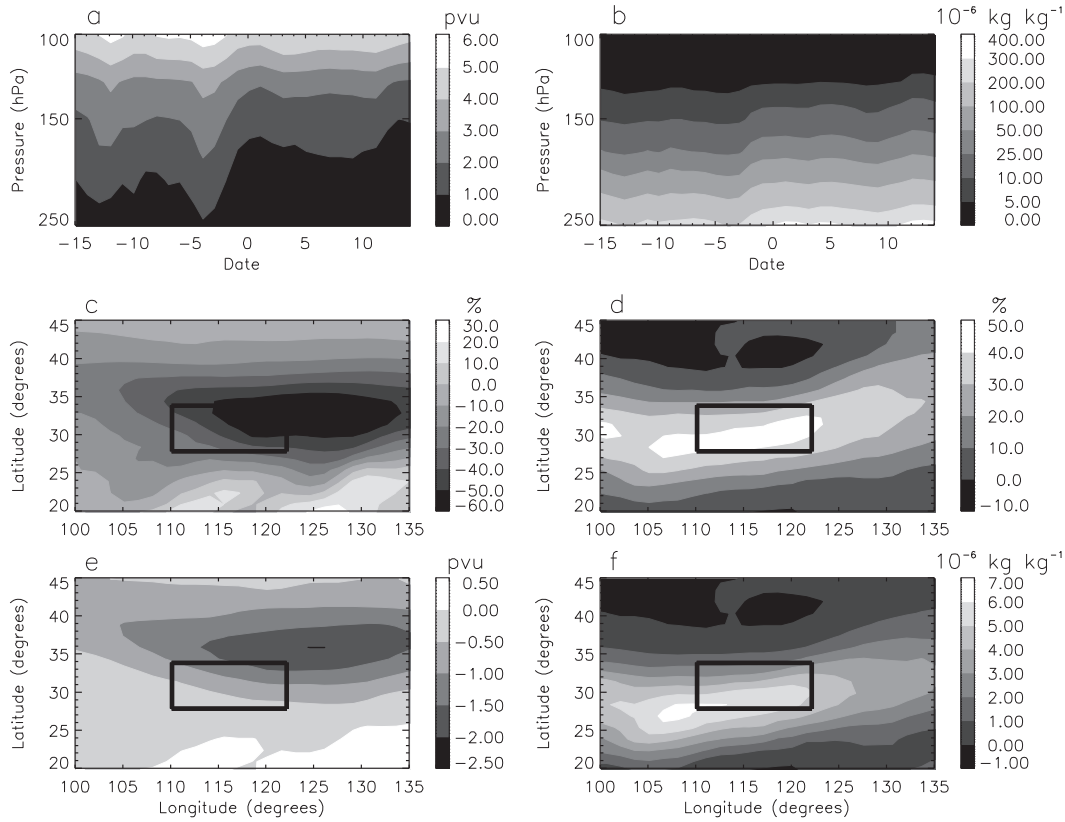

Figure 2. Time-height cross sections of (a) PV and (b) specific humidity averaged over the Meiyu region from 15 days before to 15 days after Meiyu onset. The percentage differences (see text for the definition) in (c) PV and (d) specific humidity at 150 hPa. The absolute differences in (e) PV and (f) specific humidity at 150 hPa are also given for comparison. The rectangle indicates the Meiyu region.

region of maximum specific humidity anomalies is located within the Meiyu region. Figures 2e and 2f show the absolute differences in PV and specific humidity during the Meiyu season. It is apparent that the spatial distributions of the percentage differences and the absolute differences in specific humidity and PV have overall similar features at 150 hPa.

[9] To understand this mismatch of the locations of the minimum PV and maximum water vapor in the UTLS during the Meiyu season, Figure 3a shows climatologies of the transient eddy activity during the Meiyu season measured by the standard deviation of high-frequency meridional wind at 200 hPa, calculated from a high-pass filter with a cutoff period of 8 days. The climatology of 200 hPa zonal winds is also shown in Figure 3a. It is apparent that the minima of PV anomalies are collocated

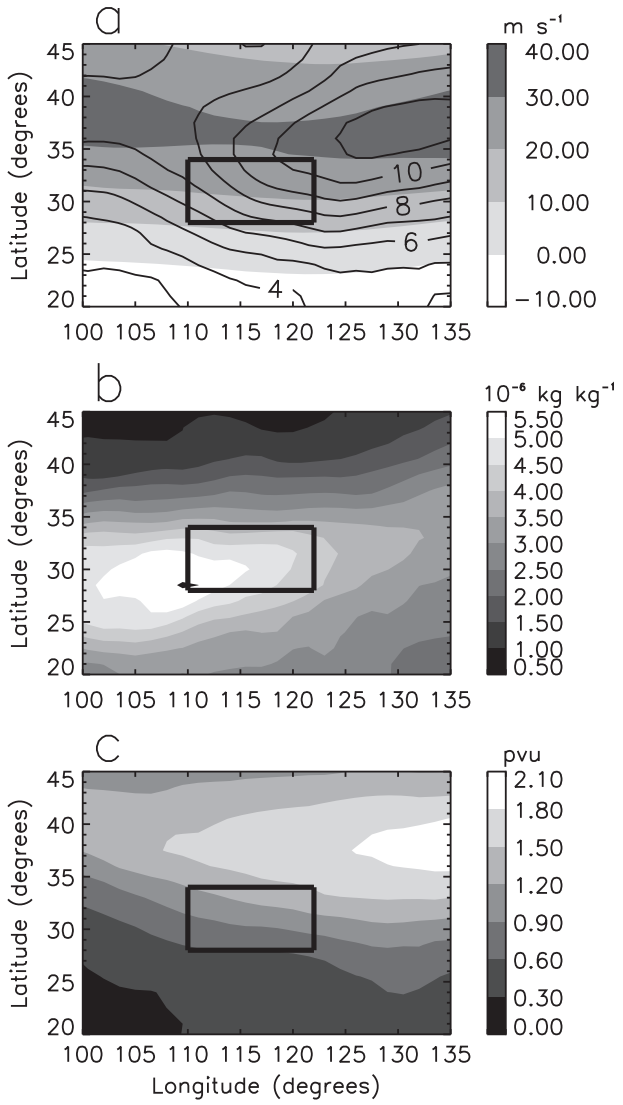

Figure 3. Climatology of root-mean-square (RMS) of high-pass-filtered (a) 200 hPa meridional wind (contour interval of 1 m s^{-1}), (b) 150 hPa specific humidity, and (c) 150 hPa PV during the Meiyu season (15 days before to 15 days after Meiyu onset). In Figure 3a, 200 hPa zonal wind speeds are also over plotted (filled contours). The rectangle indicates the Meiyu region.

with the core of the upper tropospheric westerly jet where the transient eddy activity is the strongest (Figure 3a). Previous studies [e.g., *Danielsen and Mohnen*, 1977; *Shapiro*, 1980] have found that within the core of westerly jet tropopause fold events are most likely to happen. Tropopause fold can cause significant cross tropopause mass exchange as has been evidenced in many previous studies [e.g., *Appenzeller and Davies*, 1992; *Ancellet et al*., 1991, 1994; *Vaughan et al*., 1994; *Zhang et al*., 2010]. *Holton et al*. [1995] proposed that air can be irreversibly transported as adiabatic eddy motions which lead to large latitudinal displacements of the tropopause followed by irreversible mixing on small scales in the UTLS region. On the other hand, *Sampe and Xie* [2010] stated that the midtropospheric westerlies can advect warm air from the eastern flank of the Tibetan Plateau along the jet axis, inducing ascending motion that triggers convection to form the Meiyu-Baiu rainband. Therefore, the upward transport of air from the troposphere into the stratosphere in the Meiyu region is closely related to the upper tropospheric westerly jet and transient eddy activities, and the region with strongest upward transport is located northeast of the Meiyu region. Figures 3b and 3c further show high-pass filtered 150 hPa specific humidity and PV fields during the Meiyu season (averaged over 15 days before to 15 days after Meiyu onset). It is evident that during the Meiyu season the center of the maximum water vapor anomalies at 150 hPa is located in the west of the Meiyu region, while the center of the maximum PV anomalies at 150 hPa is located to the northeast of the Meiyu region. The result here suggests that the anomaly center of specific humidity is collocated with the region with highest water vapor in the Meiyu area while anomaly center of PV is collocated with the region with the strongest upward transport.

[10] Figures 4a and 4c shows the time variations of the tropopause height and temperature averaged over the Meiyu area, respectively. It is evident that the tropopause descends between the ninth and third days before Meiyu onset. Then it soars until about the third day after Meiyu onset. The first maximum of the tropopause height occurs from 1 day after Meiyu onset and then reach the second maximum 14 days after Meiyu onset. The difference in tropopause height between its maximum and minimum can reach 1.2 km during the Meiyu season. The tropopause becomes stable from the third day to tenth day after Meiyu onset with little fluctuations in its height. As expected, the tropopause temperature drops from the third day before Meiyu onset to the second day after Meiyu onset, and the maximum temperature appears at the third day before Meiyu onset and the minimum temperature is found at the second day after Meiyu onset (Figure 4c). The time variations of tropopause height and temperature are in close accordance with the time variations of PV and water vapor fields during the Meiyu season as shown in Figures 2a and 2b. As will be shown later, the rise of tropopause after Meiyu onset reflects the enhanced convective activities and strong ascending motion of tropospheric air. Consequently, PV at 150 hPa decrease and the specific humidity increases after Meiyu onset as is evident in Figures 2a and 2b. *Zhu et al*. [2007] demonstrated convincing evidence that the ascending motion is significantly enhanced in the lower troposphere after Meiyu onset. An interesting feature in Figures 4a and 4c is

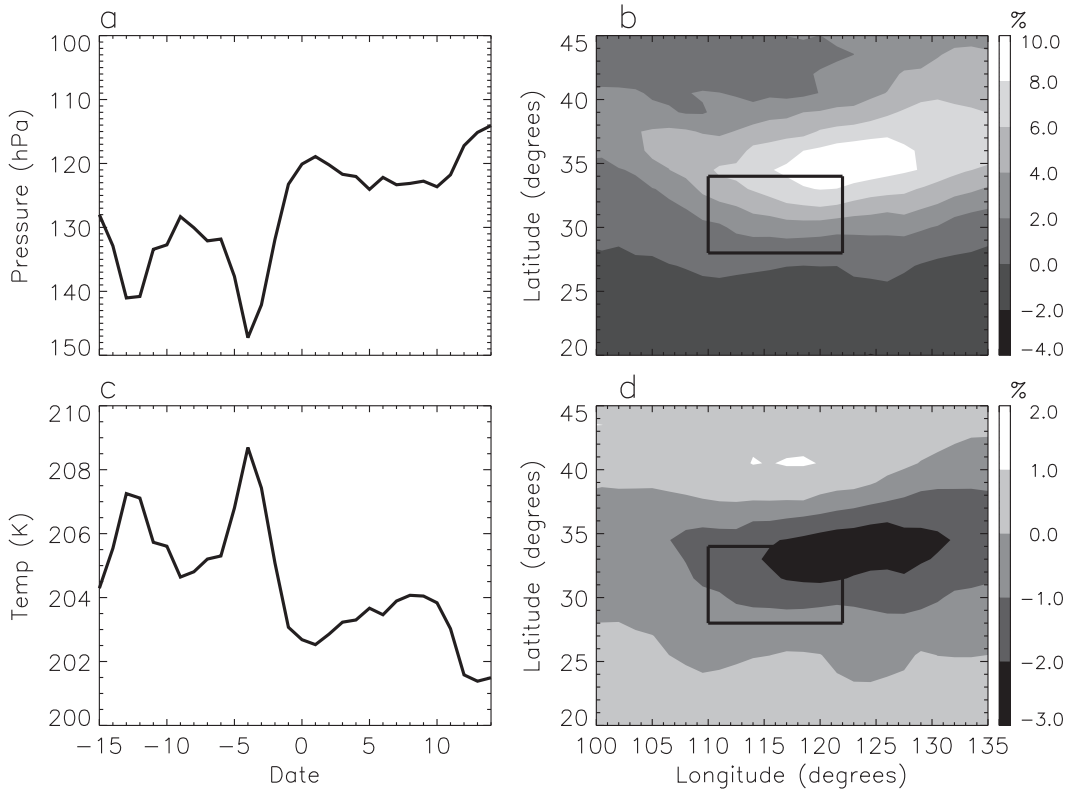

Figure 4. Time variations of (a) the tropopause height and (c) tropopause temperature from 15 days before to 15 days after Meiyu onset, averaged over the Meiyu region. The percentage differences in 15 day mean (b) tropopause height and (d) tropopause temperature before and after Meiyu onset. The rectangle indicates the Meiyu region.

the significant decrease in tropopause height and the corresponded increase in the tropopause temperature before Meiyu onset, which can be attributed to frequent tropopause fold events over the Meiyu area (see section 4). It is well known that mesoscale tropopause folds events have an important contribution to downward transport of the stratospheric air into the troposphere [e.g., *Danielsen*, 1968; *Shapiro*, 1980; *Appenzeller and Davies*, 1992; *Ancellet et al*., 1991, 1994; *Vaughan et al*., 1994; *Eisele et al*., 1999; *Kentarchos et al*., 1998, 1999; *Zhang et al*., 2010]. More tropopause fold events imply stronger downward transport of air from the stratosphere and higher PV in the upper troposphere. This speculation can be supported by Figure 2a, which indicates that PV reaches their peak values on the third day before Meiyu onset.

[11] Figures 4b and 4d further show latitude-longitude distributions of percentage changes in the tropopause height and temperature before and after Meiyu onset. Note that the minimum of tropopause height anomalies and the maximum of tropopause temperature anomalies are located at northeast of the Meiyu area (115°–130°E, 30°–36°N), consistent with distributions of anomalies in PV in the UTLS (Figure 2c). The result here confirms that the strongest upward transport is located in northeast of the Meiyu area rather than within it.

[12] It is known that radiation and baroclinic (and other) waves as well as convection can significantly affect the structure of the tropopause. We have mentioned above that tropopause variations over the Meiyu area during the Meiyu season are mainly due to convection. Figure 5 illustrates the time variation of the tropopause height over the Meiyu area in June (Meiyu mostly onsets in this month in each year) averaged over the 18 year data and the time-height cross section of tropopause and vertical velocity 15 days before to 15 days after Meiyu onset. Figure 5a shows that the variation of the climate mean tropopause in June is rather flat. This result implies that radiation forcing cannot generate significant tropopause variations shown in Figure 4. Figure 5b shows that the vertical velocity increases about 3 days before Meiyu onset, the tropopause lifts accordingly. The upward motions are strong from about 1 day before Meiyu onset to 8 days after Meiyu onset (see the shaded region in Figure 5b), i.e., vertical motions are significantly enhanced after Meiyu onset and hence a lifted tropopause.

[13] Figure 6 shows the latitude-height and longitude-height cross sections of anomalies of PV and specific humidity fields averaged over the longitude band 110°–122°E and the latitude band 28°–34°N, respectively. Large PV anomalies are clearly seen at 100–300 hPa while there are no significant PV anomalies within the Meiyu region in the lower troposphere (Figures 6a and 6b). This is understandable since the PV anomalies are mainly induced by the downward transport of high PV air from the stratosphere. In contrast, the water vapor anomalies can be seen in both the upper and lower troposphere (Figures 6c and 6d). The center of maximum water vapor anomalies is almost collocated with the Meiyu region with a seemingly

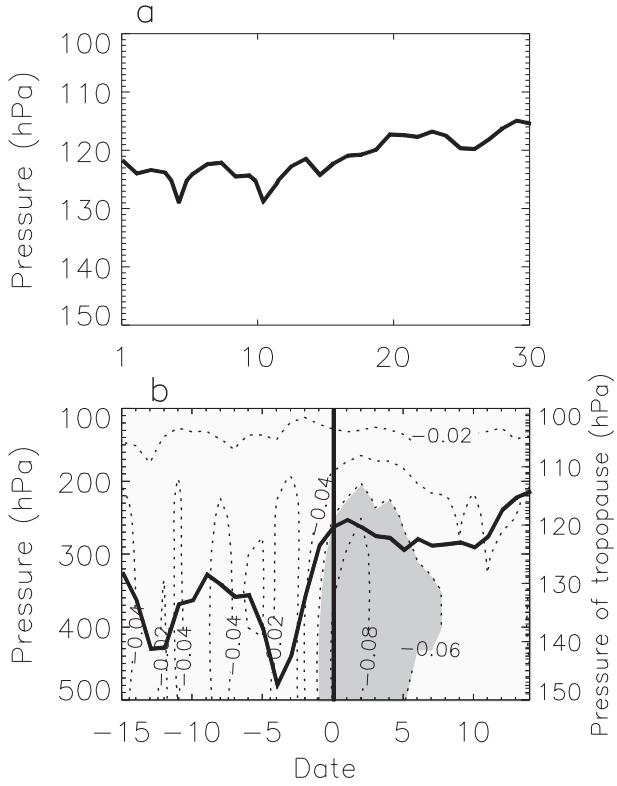

Figure 5. (a) Daily variations of the tropopause height over the Meiyu area in June averaged over the 18 years of data. (b) The time-height cross section of composited tropopause and vertical velocity. The thick black line denotes the tropopause, and the vertical black line indicates the day of Meiyu onset. The contour interval is 0.02 Pa s^{-1}. The region with vertical velocity less than -0.06 Pa s^{-1} is shaded.

southward shift of the maximum abnormal center in the upper troposphere. The minimum PV anomalies are found in the east of the Meiyu region that is possibly linked with the onset of Baiu in Japan. However, the longitude-height distributions of specific humidity differences have their maximum values in the west of the Meiyu area (Figure 6d). Again, a possible reason for different locations of maximum water vapor anomalies and minimum PV anomalies is that the water vapor anomalies have their largest source within the Meiyu region while the PV anomalies are originated from the lower stratosphere through STE processes. Also note that the minimum center of percentage differences in PV is located in the Meiyu area (Figure 6a) while minimum center of the absolute changes in PV is located north of the Meiyu area (Figure 6e). Compared to the percentage differences in specific humidity, the absolute differences in specific humidity show no significant variations within the Meiyu area due to large background values of water vapor in the lower troposphere (Figures 6 g and 6 h).

4. Variations of Cross-Tropopause Mass Flux

[14] The analysis in section 3 suggests significant downward and upward transport of air masses in the UTLS region before and after Meiyu onset, respectively. In this section we attempt to provide more details of STE processes associated with Meiyu and diagnose quantitatively the STE flux before and after Meiyu onset.

[15] Figure 7a illustrates the time variations of the cross-tropopause mass flux (CTMF) from 15 days before Meiyu onset to 15 days after Meiyu onset. The CTMF is calculated using the method proposed by *Wei* [1987]. The CTMF estimated from Wei' method consists of three components: the one accounts for the horizontal transport arising from the pressure gradient along the tropopause, the second one is associated with the vertical transport due to vertical motions at tropopause level, and the last one accounts for the exchange of mass resulting from the temporal fluctuation of tropopause pressure. In Figure 7a, the time variations of the CTMF associated with vertical and horizontal transports are overplotted with the total CTMF for comparison (the CTMF due to tropopause variations is rather small and is omitted for clarity). It is evident that the total CTMF is always negative from 15 days before to 15 days after Meiyu onset, suggesting a net downward transport of air mass from stratosphere to troposphere. However, the downward transport has an overall weakening trend from 15 days before Meiyu onset to 15 days after Meiyu onset, implying the upward cross tropopause transport is gradually increasing during the Meiyu season. Meanwhile, the time variations of the CTMF are in close accordance with the time variations of PV and water vapor fields as well as tropopause height during the Meiyu season. A large downward CTMF also exists around the third day before Meiyu onset. Previous studies indicated that air can transport from the surface into the stratosphere during the Asian monsoon season due to intensified convective activities [e.g., *Randel et al*., 2010]. Figure 7a demonstrates that the CTMF due to vertical motions is upward and becomes stronger after Meiyu onset. Although the total CTMF is still marginally negative, those negative values become smaller and smaller implying that the downward transport is weakening gradually. Meanwhile, the time variations of mass fluxes caused by horizontal transport is much close to that of the total CTMF (Figure 7a), implying the mass exchange associated with the pressure gradient along the tropopause makes the largest contribution to the total CTMF over the Meiyu region. As will be shown later in this section, due to the development of the baroclinic instability in the westerly jet and frequent the upper level frontogenesis before Meiyu onset, tropopause fold events are more likely to happen in the Meiyu region. More tropopause folds will cause more downward transport of air into the troposphere in the trough of the tropopause fold [e.g., *Cooper et al*., 2001; *Roelofs et al*., 2003]. On the other hand, tropopause folds are always accompanied with large pressure gradients along the tropopause which results in strong cross tropopause mass exchange.

[16] The above analysis reveals that the net CTMF is weakly downward within the Meiyu area although the CTMF associated with the vertical motions are upward and increases significantly after Meiyu onset. To cross-check the climate feature of the CTMF during the Meiyu season, a 30 year climate model (WACCM3) simulation from 1981 to 2010 is performed and the CTMF variations in June estimated from the model output are shown in Figure 7b. It is apparent that the modeled climate mean total CTMF in June is slightly positive and exhibits no significant trend of

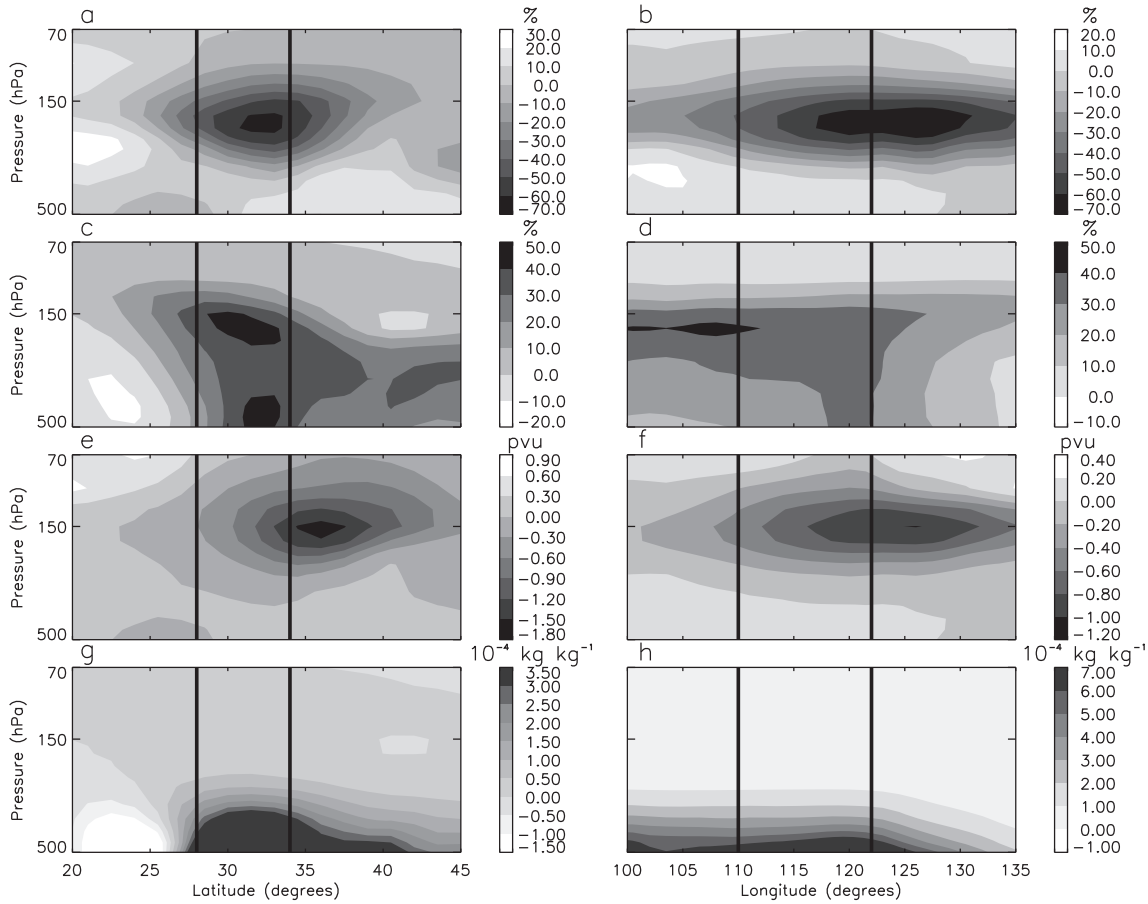

Figure 6. (a and c) Latitude-height (averaged over the longitude band 110°–122°E) and (b and d) longitude-height (averaged over the latitude band 28°–34°N) cross sections of percentage differences in PV (Figures 6a and 6b) and specific humidity (Figures 6c and 6d). The corresponding absolute differences in (e and f) PV and (g and h) specific humidity are also given for comparison. The two lines in each panel outline the boundaries of the Meiyu area.

increases in the CTMF in June. Particularly interesting is that the modeled total CTMF is exactly in phase with the CTMF associated with vertical motions while the composited total CTMF is in phase with the CTMF associated with the tropopause pressure gradient. This result manifests that the large downward cross tropopause transport associated with frequent mesoscale tropopause events just before the Meiyu season cannot be properly solved by the climate model. It should also be pointed out that the data from the climate model cannot make day-to-day comparisons with the reanalysis data while the composited CTMF variations in Figure 7a are based on daily analysis. Consequently, Figure 7b shows no evident increases in the modeled total CTMF in June. Figures 7c and 7d further show the horizontal distributions of CTMF averaged over 15 days before and after Meiyu onset, respectively. Note that a belt of strong downward CTMF covers the Meiyu region before Meiyu onset, in accordance with the distributions of anomalies of PV and water vapor shown in Figures 2c and 2d. After Meiyu onset, the belt of strong downward CTMF shifts northward out of the Meiyu region.

[17] More details of cross tropopause transport can be seen in Figures 8a and 8b in which latitude-height cross sections of the 15 day mean PV field and wind vectors (averaged over the longitude band 110°–122°E) before and after Meiyu onset are displayed. It is clear that the tropopause pressure meridional gradient over the Meiyu region is the larger before Meiyu onset while the largest meridional gradient in tropopause pressure is to the north of the Meiyu region after Meiyu onset. The sharp meridional gradient of tropopause pressure enhances the exchanges of air masses in both directions along the tropopause surface. Figure 8a suggests that the total CTMF during the Meiyu season is mainly caused by the horizontal exchange of mass along the tropopause. Figures 8a and 8b also indicate that the air flows from the stratosphere to the troposphere before Meiyu onset over the latitude band 31°–37°N where meridional gradient of the tropopause pressure is sharp (Figure 8a), implying an isentropic transport from the stratosphere to the troposphere. After Meiyu onset, the strong ascending motion can be seen in the Meiyu region, the center of the largest meridional gradients of the tropopause pressure displaces northward to about 37°N and the air flows from the stratosphere to the troposphere between 36°–38°N (Figure 8b). This is in accordance with Figure 7c, which also indicates that the center of the maximum CTMF displaces northward after Meiyu

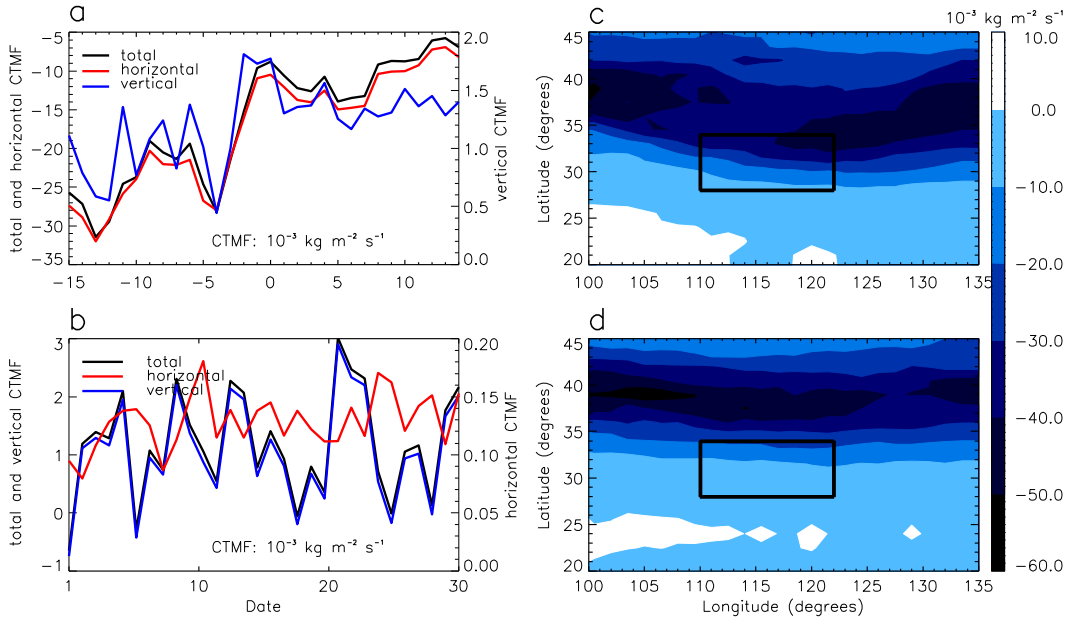

Figure 7. (a) Composited time variations of the cross-tropopause mass fluxes (CTMF; units of 10^{-3} kg m^{-2} s^{-1}) estimated from ERA-Interim data from 15 days before Meiyu onset to 15 days after Meiyu onset, averaged over the Meiyu region. (b) Climate mean time variations of the modeled CTMF in June, averaged over the Meiyu region. The black, red, and blue lines represent the total CTMF, the CTMF associated with horizontal transport, and the CTMF associated with vertical transport, respectively. The horizontal distributions of the 15 day mean total CTMF estimated from ERA-Interim data (c) before and (d) after Meiyu onset. The rectangle indicates the Meiyu region.

onset. Note that the potential temperature contours and the tropopause surface are nearly perpendicular in the UTLS around the area with the largest gradient of the tropopause pressure and the isentropic surfaces intersect the tropopause, implying that the exchange of air along the isentropic surface between the troposphere and stratosphere is more likely to occur. The total CTMF is nearly upward from the troposphere to stratosphere after Meiyu onset, which is the result of strong ascending motions together with enhanced isentropic transport across the tropopause (Figure 8b). Figures 8c and 8d show longitude-height cross sections of the 15 day mean PV field and wind vectors averaged over the longitude band 28°–34°N before and after Meiyu onset, respectively. The tropopause between 120°–130°E is lower than that over surrounding regions before Meiyu onset, and the contours of PV show sinking trends in the upper troposphere over the Meiyu region and the area to the east of the Meiyu region. The tropopause is nearly flat after Meiyu onset due to strong convective motions over the Meiyu area.

[18] To understand the large CTMF on the third day before Meiyu onset, analogous to Figure 8, Figure 9 shows latitude-height and longitude-height cross sections of PV and wind vectors on the third day before and the third day after Meiyu onset. It is apparent that the center of largest meridional gradient of the tropopause pressure is located within the Meiyu region on the third day before Meiyu onset and tropopause fold-like structure can be seen in the zonal distributions of tropopause (Figures 9a and 9c). The tropopause over the Meiyu region is much lower than that over surrounding regions on the third day before Meiyu onset (Figure 9c), while the tropopause is lifted due to strong convective motions on the third day after Meiyu onset (Figure 9d). As mentioned earlier, the tropopause deformation can cause irreversible transport of air cross the tropopause. On the other hand, the sinking of the tropopause before Meiyu onset can cause an upward CTMF while the rising of the tropopause after Meiyu onset will give rise to a downward CTMF, although the CTMF associated with tropopause movements is rather small. The strong meridional gradient of the tropopause pressure together with prominent tropopause folds give rise to a large downward CTMF on the third day before Meiyu onset. After Meiyu onset, the tropopause within the Meiyu region is lifted and becomes flat both in meridional and zonal directions and the center of largest meridional gradients of the tropopause pressure displaces northward to about 37°N. In accordance with Figure 8, the ascending motion in the Meiyu region on the third day after Meiyu onset is much stronger than that on the third day before Meiyu onset.

5. Trajectory Analysis of STE

[19] The composite analysis above provides the bulk properties of the STE during the Meiyu season. In order to further verify the aforementioned conclusions, the trajectory data from the HYSPLIT (Hybrid Single-Particle Lagrangian Integrated Trajectory) model are analyzed. The HYSPLIT model assumes a three-dimensional particle distribution [*Draxler and Hess*, 1997] and air parcels are transported by the three-dimensional winds from NCEP/NCAR global reanalysis data. It should be pointed out that the wind fields from NCEP/NCAR and ERA-Interim two data sets

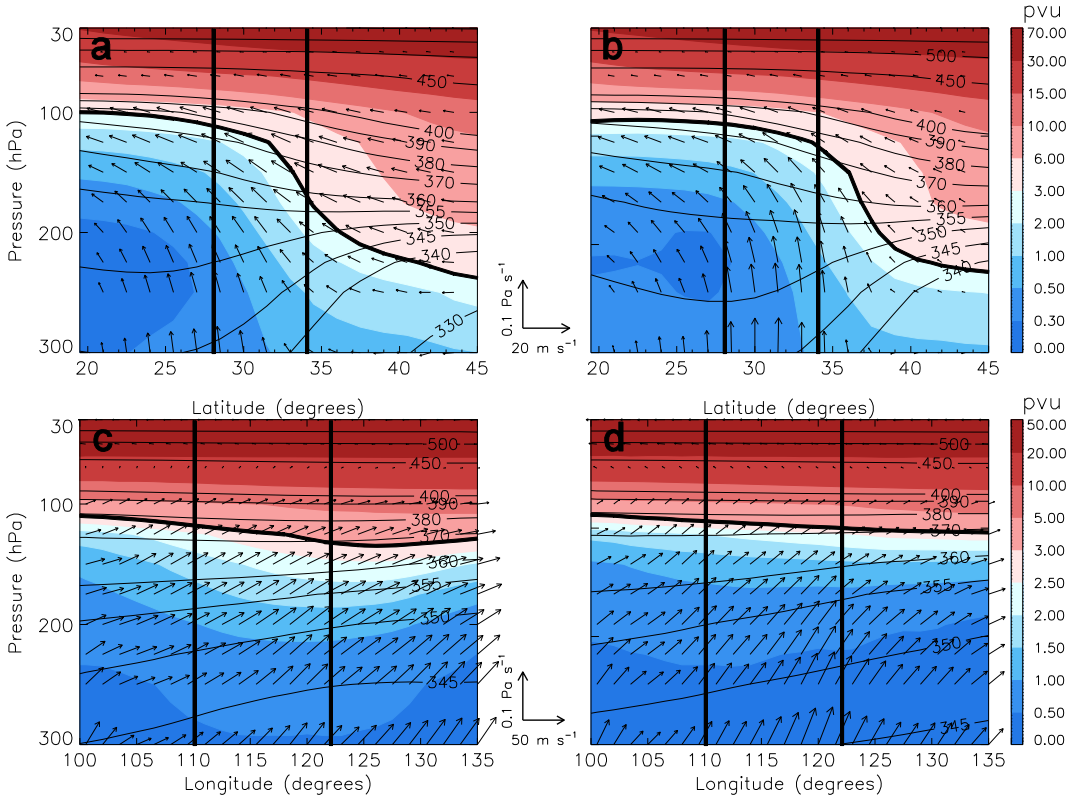

Figure 8. (a and b) Latitude-height (averaged over the longitude band 110°–122°E) and (c and d) longitude-height (averaged over the latitude band 28°–34°N) cross sections of the mean PV fields 15 days (left) before and (right) after Meiyu onset. The thick black line denotes the tropopause. The thin black lines are potential temperature contours (K). The arrows indicate wind vectors (unit of zonal and meridional wind is m s^{-1}; unit of vertical wind is Pa s^{-1}). The PV fields are represented by color contours. The two vertical lines in each panel outline the boundaries of the Meiyu area.

have a good accordance within the study area (not shown). Given that analysis based on individual trajectories may have uncertainties, we used an ensemble approach to do the analysis. The ensemble approach starts multiple trajectories from a selected starting location. Each trajectory in the approach is calculated by offsetting the meteorological data by a fixed grid factor. The approach results in 27 trajectories for all possible offsets in three directions [*Draxler et al.*, 2012]. We chose four different heights to analyze the trajectories of air parcels during the Meiyu season, including trajectories at 8, 10, 12, and 15 km. Figure 10 shows the time-height distributions of the backward and forward trajectories at the four heights from 1989 to 1997. Also demonstrated in Figure 10 are the time variations of dynamical tropopause heights averaged over the Meiyu region during the trajectory running periods. For consistency, the tropopause heights derived from the NCEP reanalysis data are plotted here. The day of Meiyu onset in each year is chosen as the reference time and the departure point is at 30°N, 115°E. The trajectories are then calculated 10 days before (backward) and after (forward) Meiyu onset. The backward trajectories of the air parcel at 12 km (Figure 10e) and 15 km (Figure 10 g) show that the air is transported from the upper levels to the troposphere from 3 to 5 days before Meiyu onset, and then it is transported toward the stratosphere 1 day before Meiyu onset. Note that the tropopause heights within the Meiyu region during the running time of the trajectories fluctuate at round 12 km with a maximum of no more than 14 km (Figures 10i and 10j). Figure 10 clearly suggests that the air of stratospheric origin intrudes into the troposphere before Meiyu onset. Figures 10a and 10c indicate that air parcels in the middle troposphere have no contacts with the air in upper levels and air parcels in the upper troposphere showed a relatively weaker downward trend before Meiyu onset. The forward trajectories at 8 km (Figure 10b) show evident upward movement of air parcels after Meiyu onset. The upward movements of air parcels at 10 km (Figure 10d) and near the tropopause (Figure 10f) are less significant than those at the lower levels, but a slow and long-lasting movement can be observed. The upward movement of the air parcels at 15 km can still be noted (Figure 10 h), but no upward movements are found from the trajectories at 18 km (not shown).

[20] It has been recognized that the circulations associated with Meiyu have significant interannual variations [e. g., *Krishnan and Sugi*, 2001; *Qian et al.*, 2009; *Si et al.*, 2009]. Figure 10 indicates that the trajectories during the Meiyu season vary year by year. To provide more details of transport of air masses between the stratosphere and the troposphere before and after Meiyu over the Yangtze-Huaihe Valley, we first divide Meiyu years into two categories based on the intensity of precipitation during the Meiyu season in each year, i.e., rich Meiyu years and poor Meiyu years.

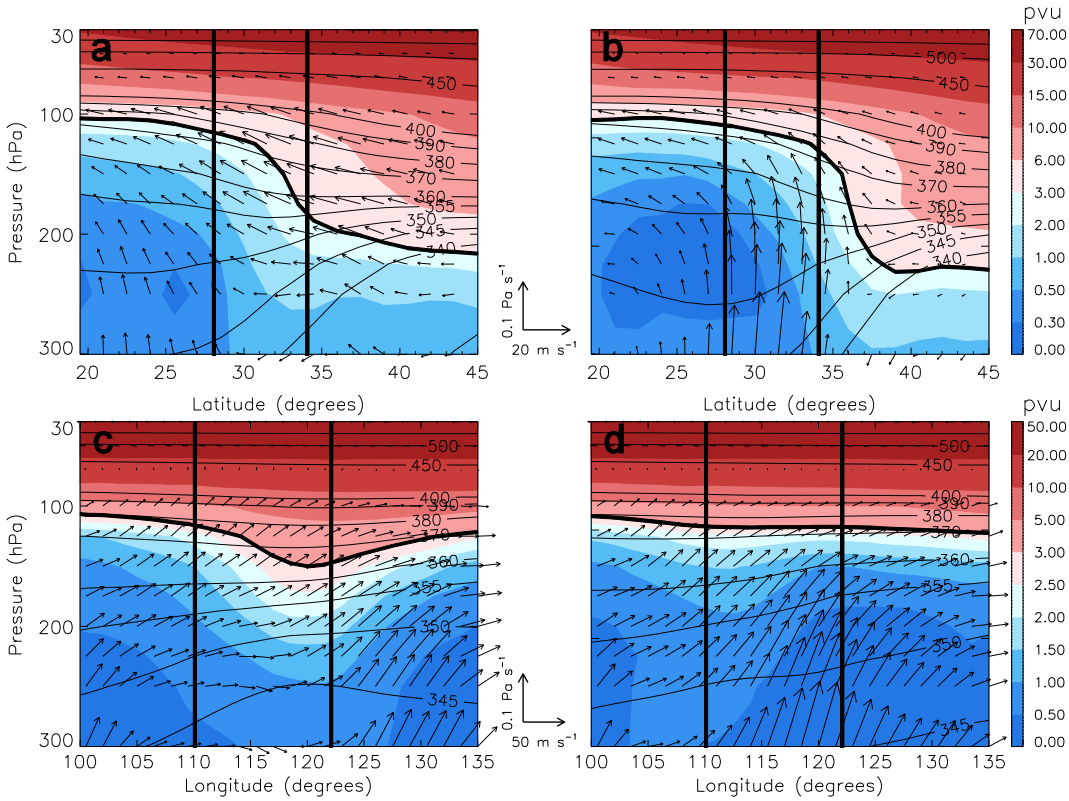

Figure 9. Same as Figure 8, except for latitude-height cross sections of PV (pvu) fields on the third day (a) before and (b) after Meiyu onset (averaged over the longitude band 110°–122°E) and longitude-height cross sections of PV fields averaged over the latitude band 28°–34°N on the third day (c) before and (d) after Meiyu onset.

According to the precipitation records from the National Climate Center of China, the average intensity of precipitation during Meiyu seasons between 1971 and 2000 is 63 mm d^{-1}. The year 1999 is selected as a typical rich Meiyu year as it has a precipitation of 211 mm d^{-1} during the Meiyu season, while the year 2005 is selected as a typical poor Meiyu year since it has a small precipitation 48 mm d^{-1} during the Meiyu season. Figure 11 compares the forward trajectories in 2005 and 1999 initiated at different locations around the Meiyu area. It is apparent that the forward trajectories in 1999 (rich Meiyu year) initiated at 10 km show significant upward movements and can get into the lower stratosphere (Figure 11b), while the forward trajectories in 2005 (poor Meiyu year) initiated at 10 km show no significant upward movements and the air parcels initiated at 10 km reach a height of no more than 14 km which is below the tropopause (Figure 11a). The forward trajectories initiated at 12 km in 1999 also show significant upward movements after Meiyu onset. The trajectories initiated at the south of the Meiyu region can reach a height of about 16 km, well into the stratosphere (Figure 11d). The upward movement of the forward trajectories initiated at 12 km in 2005 is less significant and they even show downward movements between the second day and fourth day after Meiyu onset (Figure 11c). Above 15 km, differences in trajectories between 2005 and 1999 are still significant (not shown). As expected, the net CTMF in the Meiyu region was weaker in year 1999 than that in year 2005 and water vapor around 150 hPa in 1999 was more abundant than that in year 2005 (not shown). It is evident from Figure 11 that the trajectories initiated at the south of the Meiyu region show a relatively strong upward transport in the rich Meiyu year, while trajectories initiated at the north of the Meiyu area show a relatively weak upward transport. This is mainly due to that South Asia Monsoon brings up more and stronger convective activities to the south of the Meiyu region. In contrast, trajectories in year 2005 had no such a feature. Particularly noticeable is that in 2005 the trajectories initiated at the north of the Meiyu area can even reach a higher altitude than the trajectories initiated at the south of the Meiyu area.

[21] The above analysis is based on the mean value of 27 ensemble trajectories. To further verify the results shown in Figures 10 and 11, the ensemble trajectory analysis of each trace is performed for the case of 1999 Meiyu season. With the same departure point and the reference time as in Figure 10, Figure 12 shows the cluster of backward and forward trajectories initiated at four heights 5 days before and after Meiyu onset. Note that in the middle troposphere (8 km, Figure 12a), the backward trajectories all have the same horizontal pathway approaching from the west of the Meiyu region. In the vertical, some of those trajectories come from an altitude of about 10 km while the majority of them come from lower levels below 8 km. The forward trajectories at 8 km show consistent upward movements with some of them reaching to a height of 13.5 km (Figure 12b). Also note that after Meiyu onset, air at 8 km within the

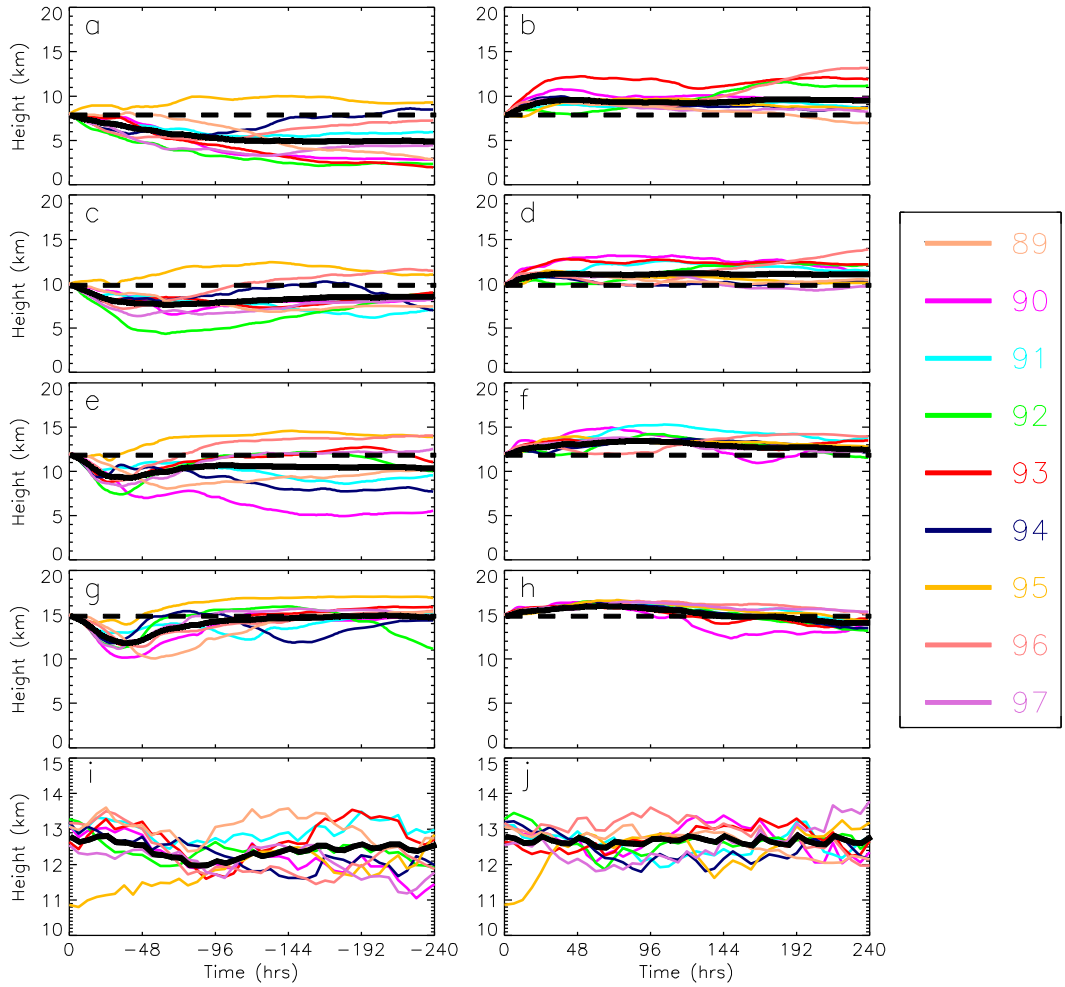

Figure 10. The time-height variations of (Figures 10a, 10c, 10e, and 10g) backward and (Figures 10b, 10d, 10f, and 10h) forward trajectories at (a and b) 8 km, (c and d) 10 km, (e and f) 12 km, and (g and h) 15 km in years from 1989 to 1997. The day of Meiyu onset was chosen as the reference time, and the trajectories are 10 days before and after it. The departure point is at 30°N, 115°E. The dashed lines indicate 8, 10, 12, and 15 km, respectively. The time variations of dynamical tropopause heights averaged over the Meiyu region during the (i) backward and (j) forward trajectory running periods are also shown for reference. Different colors correspond to trajectories and tropopause heights in different years. The thick black line in each panel indicates the 9 year averaged trajectories (Figures 10a–10h) and tropopause heights (Figures 10i and 10j). Each trajectory is derived from the mean of 27 ensemble trajectories.

Meiyu region move both toward the west of the Meiyu region and East Asia Monsoon region.

[22] In the upper troposphere (10 km, Figure 12c), backward trajectories also all come from the west of the Meiyu region and most of them show downward movements 3 days before Meiyu onset. The forward trajectories show persistent upward movements until 4 days after Meiyu onset, reaching a height of 14.5 km implying that the air parcels are transported into the UTLS within the Meiyu region after Meiyu onset (Figure 12d). The horizontal pathway of forward trajectories at 10 km is similar as that at 8 km, but more trajectories move toward northwest of the Meiyu region.

[23] The backward trajectories initiated at around the tropopause (12 km, Figure 12e) show that air parcels also come from the west of the Meiyu region and move downward 3 days before Meiyu onset. The forward trajectories show upward movements after Meiyu onset and some trajectories can reach a height of more than 15 km (Figure 12f). As the tropopause height is about 12 km within the Meiyu region, the result confirms that the air in the Meiyu region is transported into the stratosphere after Meiyu onset. The majority of forward trajectories push toward northwest of the Meiyu region and some others approach toward northeast of the Meiyu region.

[24] The backward trajectories initiated at the lower stratosphere (15 km, Figure 12 g) show significant downward movement 3 days before Meiyu onset suggesting the prominent intrusion of the stratospheric air into the troposphere, while forward trajectories show significant upward movements of air parcels after Meiyu onset reaching a level of around 17 km (Figure 12 h). It is also worth to note that the forward trajectories at 15 km all have the same horizontal path way to

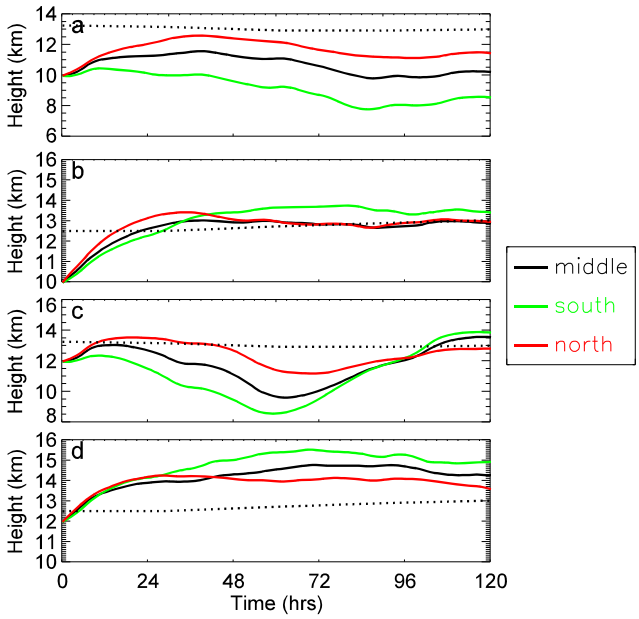

Figure 11. The forward trajectories at (a and b) 10 km and (c and d) 12 km in 2005 (Figures 11a and 11c) and 1999 (Figures 11b and 11d). The trajectories are initiated at three different locations, i.e., at the center of the Meiyu area (31°N, 116°E; black line), at the south of the Meiyu area (28°N, 116°E; green line), and at the north of the Meiyu area (34°N, 116°E; red line). The dashed line in each panel represents the time variation of dynamical tropopause heights averaged over the Meiyu region during the trajectory running periods. Each trajectory is derived from the mean of 27 ensemble trajectories.

the west of the Meiyu region, in contrast with the trajectories initiated at 8, 10, and 12 km.

[25] Figure 13 further illustrates the zonal winds at 200 hPa averaged over the Meiyu season (from 15 days before to 15 days after Meiyu onset) in 2005 and 1999. It is clear that the upper level westerly jet in 2005 was weaker than in 1999. In 2005, westerly wind speed was less than 30 m s^{-1}, while it exceeds 30 m s^{-1} in east of 130°E and west of 100°E over the Meiyu region (Figure 13a). In 1999, the axis of the upper level westerly jet was located north of the Meiyu region (35°–45°N; Figure 13b) and consistent with the result from the composite analysis presented in Figure 3. In the poor Meiyu year 2005, the axis of the upper level westerly jet was located far from the Meiyu area (Figure 13a). When westerly jet is weak in poor Meiyu years, the transient eddies and upward motions are weak, implying weak upward transport cross the tropopause, and this result can also be supported by the fact that there is less water vapor at 150 hPa over the Meiyu region in the poor Meiyu year than in the rich Meiyu year (not shown).

6. Conclusions

[26] Using the 6-hourly ERA-Interim reanalysis products, NCEP/NCAR reanalysis data, Meiyu data from the National Climate Center of China, a GCM and a trajectory model, characteristics of stratosphere-troposphere exchange during the Meiyu season are examined in this study. The increases of PV and the decreases in specific humidity in the UTLS region before Meiyu onset suggest strong downward transport of air masses around the tropopause. It is found that the maximum center of specific humidity anomalies associated with Meiyu is not collocated with the minimum center of PV anomalies. The region with maximum specific humidity is located in the Meiyu region, while the minimum PV is located northeast of the Meiyu region. The result indicates that the strongest upward transport in the UTLS region caused by the Meiyu occurs at northeast of the Meiyu region, just within the core of the upper tropospheric westerly jet, where the transient eddy activity is also the strongest. The water vapor anomalies within the Meiyu region are the largest mainly because the specific humidity in the lower and upper troposphere within the Meiyu region is higher than that of surrounding region during the Meiyu season. The time variations of height and temperature of tropopause over the Meiyu region reflect enhanced convective activities and strong ascending motion of tropospheric air after Meiyu onset. An interesting feature is a sharp drop of tropopause height and a peak value downward CTMF on the third day before Meiyu onset, then the tropopause lifts accompanied by stronger upward motions. The sinking of the tropopause and enhancement of the downward cross tropopause transport are thought to be associated with the frequent tropopause fold events before Meiyu onset as well as the strong horizontal exchange of air mass along the tropopause resulting from intensified meridional gradient in the tropopause pressure.

[27] The net transport within the Meiyu region is from the stratosphere to the troposphere during the Meiyu season. The exchange along the tropopause, resulting from the sharp pressure gradient makes the largest contribution to the total CTMF. The location of the largest meridional gradient in the tropopause pressure moves northward out of the Meiyu region and the ascending motion over the Meiyu region becomes stronger after Meiyu onset. Consequently, the center of the strongest downward transport from the stratosphere to the troposphere displaces northward after Meiyu onset.

[28] The result from a trajectory model shows that the stratospheric air from levels above 15 km intrudes into the troposphere before Meiyu onset. The downward movement of air parcel is more evident in the lower stratosphere than that near the tropopause and in the upper troposphere. Significant upward movements of air parcels in the middle troposphere are notable after Meiyu onset. The upward movement of air parcels near the tropopause is relatively slow but long-lasting. As convective activities are weaker and the upper level westerly jet is located far from the Meiyu area in poor Meiyu years, the upward CTMF over the Meiyu region is accordingly weaker during the Meiyu season. The trajectory analysis also reveals that the middle and upper tropospheric air which can be transported into the upper level within the Meiyu region have different horizontal pathways while the air intrudes into the troposphere within the Meiyu region before Meiyu onset follows the same pathway. The upward transport of air parcels at the south of the Meiyu region is relatively stronger than that at the north of the Meiyu area in the rich Meiyu year.

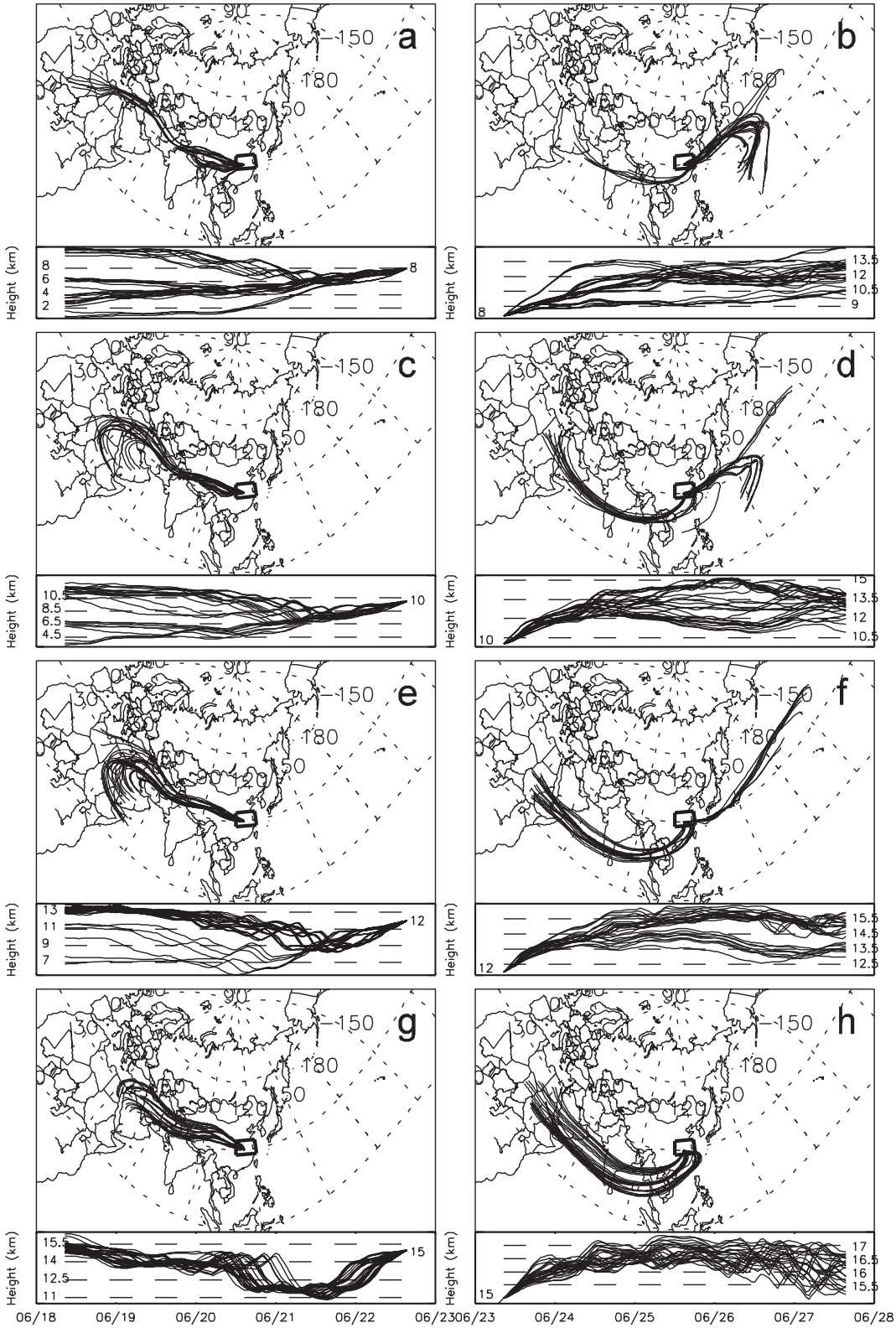

Figure 12. The ensemble backward trajectories on (a) 8 km , (c) 10 km, (e) 12 km, and (g) 15 km and forward trajectories on (b) 8 km, (d) 10 km, (f) 12 km, and (h) 15 km in 1999. The top part of the each panel shows the time evolution of trajectories in the horizontal, and the bottom part of the each panel shows the vertical variation of trajectories with time. The day of the Meiyu onset is chosen as the beginning time, and the trajectories are 5 days before and after it. The departure point is at 30°N, 115°E. The rectangle in each panel indicates the Meiyu region.

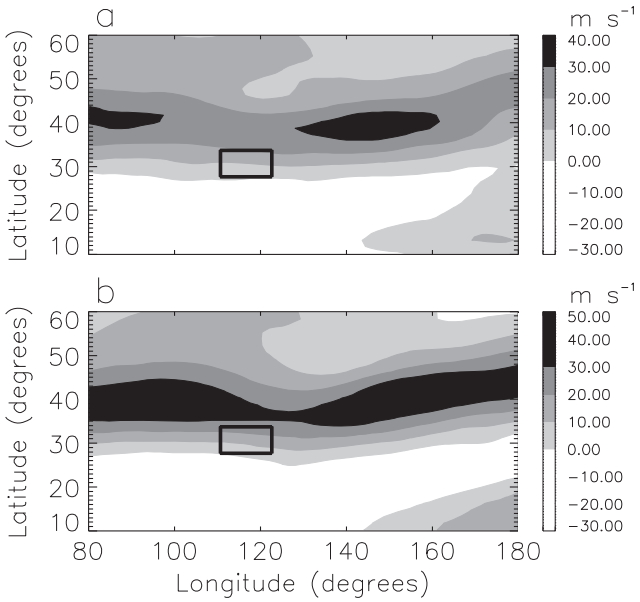

Figure 13. Mean zonal wind averaged over the Meiyu season (15 days before to 15 days after its onset) at 200 hPa in (a) 2005 and (b) 1999. The rectangle indicates the Meiyu region.

[29] **Acknowledgments.** This work was supported by the National Basic Research Program of China (2010CB428604), the National Science Foundation of China (41175042, 41225018), and the Fundamental Research Funds for the Central Universities of China (lzujbky-2012-k04). We would also like to thank ECMWF/NCEP for meteorological data and NCAR for providing the WACCM model. We also thank three anonymous reviewers for their helpful comments.

References

Ancellet, G., J. Pelon, M. Beekmann, A. Papayannis, and G. Megie (1991), Ground based lidar studies of ozone exchanges between the stratosphere and the troposphere, *J. Geophys. Res.*, *96*, 22,401–22,421.

Ancellet, G., M. Beekmann, and A. Papayannis (1994), Impact of a cutoff low development on downward transport of ozone in the troposphere, *J. Geophys. Res.*, *99*, 3451–3468.

Appenzeller, C., and H. C. Davies (1992), Structure of stratospheric intrusions into the troposphere, *Nature*, *358*, 570–572.

Chen, G. T. J., C. C. Wang, and S. C. S. Liu (2003), Potential vorticity diagnostics of a Mei-Yu front case, *Mon. Weather Rev.*, *131*, 2680–2696.

Cooper, O. R., J. L. Moody, D. D. Parrish, M. Trainer, T. B. Reyrson, J. S. Holloway, G. Hübler, F. C. Fehsenfeld, S. J. Oltmans, and M. J. Evans (2001), Trace gas signatures of the airstreams within North Atlantic cyclones: Case studies from the North Atlantic Regional Experiment (NARE '97) aircraft intensive, *J. Geophys. Res.*, *106*, 5437–5456.

Danielsen, E. F. (1968), Stratospheric-tropospheric exchange based upon radio-activity, ozone, and potential vorticity, *J. Atmos. Sci.*, *25*, 502–518.

Danielsen, E. F., and V. A. Mohnen (1977), Project duststorm report: Ozone transport, in situ measurements, and meteorological analyses of tropopause folding, *J. Geophys. Res.*, *82*, 5867–5877.

Ding, Y. H. (1991), Monsoon Over China, 419 pp., Kluwer Acad., Dordrecht, Netherlands.

Draxler, R., and G. D. Hess (1997), Description of the HYSPLIT_4 modeling system, *NOAA Tech. Memo. ERL ARL-224*, NOAA, Silver Spring, Md.

Draxler, R., B. Stunder, G. Rolph, A. Stein, and A. Taylor (2012), HYSPLIT4 user's guide, http://www.arl.noaa.gov/documents/reports/hysplit_user_guide.pdf, last revision: March, 2012.

Eisele, H., H. E. Scheel, R. Sladkovic, and T. Trickl (1999), High-resolution lidar measurements of stratosphere- troposphere exchange, *J. Atmos. Sci.*, *56*, 319–330.

Fu, R., Y. Hu, J. S. Wright, J. H. Jiang, R. E. Dickinson, M. Chen, M. Filipiak, W. G. Read, J. W. Waters, and D. L. Wu (2006), Short circuit of water vapor and polluted air to the global stratosphere by convective transport over the Tibetan Plateau, *Proc. Natl. Acad. Sci. U. S. A.*, *103*, 5664–5669.

Garcia, R. R., D. R. Marsh, D. E. Kinnison, B. A. Boville, and F. Sassi (2007), Simulation of secular trends in the middle atmosphere, 1950–2003, *J. Geophys. Res.*, *112*, D09301, doi:10.1029/2006JD007485.

Gettleman, A., D. E. Kinnison, T. J. Dunkerton, and G. P. Brasseuret (2004), Impact of monsoon circulations on the upper troposphere and lower stratosphere, *J. Geophys. Res.*, *109*, D22101, doi:10.1029/2004JD004878.

Holton, J. R., P. H. Haynes, M. E. Mclntyre, A. R. Douglass, R. B. Rood, and L. Pfister (1995), Stratosphere-troposphere exchange, *Rev. Geophys.*, *33*(4), 403–439.

Hu, Y., Y. H. Ding, and F. Liao (2008), A study of updated definition and climatological characters of Meiyu season in the Yangtze-Huaihe region [in Chinese], *Sci. Atmos. Sin.*, *32*(1), 101–112.

Kawatani, Y., and M. Takahashi (2003), Simulation of the Baiu Front in a high resolution AGCM, *J. Meteorol. Soc. Jpn.*, *81*, 113–126.

Kentarchos, A. S., T. D. Davies, and C. S. Zerefos (1998), A low latitude stratospheric intrusion associated with a cut-off low, *Geophys. Res. Lett.*, *25*, 67–70.

Kentarchos, A. S., G. J. Roelofs, and J. Lelieveld (1999), Model study of a stratospheric intrusion event at lower midlatitudes associated with the development of a cutoff low, *J. Geophys. Res.*, *104*(D1), 1717–1727.

Krishnan K., and M. Sugi (2001), Notes and correspondence Baiu rainfall variability and associated monsoon teleconnections, *J. Meteorol. Soc. Jpn.*, *79*, 851–860.

Liang, X. Z., and W. C. Wang (1998), Associations between China monsoon rainfall and tropospheric jets, *Q. J. R. Meteorol. Soc.*, *124*, 2597–2623.

Moteki, Q., T. Shinoda, S. Shimizu, S. Maeda, H. Minda, K. Tsuboki, and H. Uyeda (2006), Multiple frontal structure in the Baiu frontal zone observed by aircraft on 27 June 2004, *SOLA*, *2*, 132–135.

Ninomiya, K. (2000), Large- and meso-alpha-scale characteristics of Meiyu-Baiu front associated with intense rainfalls in 1–10 July 1991, *J. Meteorol. Soc. Jpn.*, *78*, 141–157.

Ninomiya, K. (2001), Large l-shaped cloud zone formed around 6 July 1991 with pole-ward moisture transport from intense rainfall area in Meiyu-Baiu front, *J. Meteorol. Soc. Jpn.*, *79*, 805–813.

Ninomiya, K., and T. Akiyama (1992), Multi-scale features of Baiu, the summer monsoon over Japan and the East Asia, *J. Meteorol. Soc. Jpn.*, *70*, 467–495.

Ninomiya, K., and T. Murakami (1987), The early summer rainy season (Baiu) over Japan, in Monsoon Meteorology, edited by P.-C. Chang and T. N. Krishnamurti, pp. 93–121, Oxford Univ. Press, Oxford, U. K.

Ninomiya, K., and Y. Shibagaki (2007), Multi-scale features of the Meiyu-Baiu front and associated precipitation systems, *J. Meteorol. Soc. Jpn.*, *85B*, 103–122.

Park, M., W. J. Randel, D. E. Kinnison, R. R. Garcia, and W. Choi (2004), Seasonal variation of methane, water vapor, and nitrogen oxides near the tropopause: Satellite observations and model simulations, *J. Geophys. Res.*, *109*, D03302, doi:10.1029/2003JD003706.

Qian, W. H., J. Zhu, Y. G. Wang, and J. L. Fu (2009), Regional relationship between the Jiang-Huai Meiyu and the equatorial surface-subsurface temperature anomalies, *Chin. Sci. Bull.*, *54*, 113−119.

Randel, W. J., M. Park, L. Emmons, D. Kinnison, P. Bernath, K. A. Walker, C. Boone, and H. Pumphrey (2010), Asian monsoon transport of pollution to the stratosphere, *Science*, *328*, 611–613.

Rayner, N. A., P. Brohan, D. E. Parker, C. K. Folland, J. J. Kennedy, M. Vanicek, T. Ansell, and S. F. B. Tett (2006), Improved analyses of changes and uncertainties in sea surface temperature measured in situ since the mid-nineteenth century: The HadSST2 data set, *J. Clim.*, *19*, 446–469.

Roelofs, G. J., et al. (2003), Intercomparison of tropospheric ozone models: Ozone transport in a complex tropopause folding event, *J. Geophys. Res.*, *108*(D12), 8529, doi:10.1029/2003JD003462.

Sampe, T., and S.-P. Xie (2010), Large-scale dynamics of the Meiyu–Baiu rainband: Environmental forcing by the westerly jet, *J. Clim.*, *23*, 113–134.

Shapiro, M. A. (1980), Turbulent mixing within tropopause folds as a mechanism for the exchange of chemical constituents between the stratosphere and the troposphere, *J. Atmos. Sci.*, *37*, 994–1004.

Si, D., Y. H. Ding, and Y. J. Liu (2009), Decadal northward shift of the Meiyu belt and the possible cause, *Chin. Sci. Bull.*, *54*, 4742−4748.

Tao, S., and L. Chen (1987), A review of recent research on the East Asia summer monsoon over China, in Monsoon Meteorology, edited by P.-C. Chang and T. N. Krishnamurti, pp. 50–92, Oxford Univ. Press, Oxford, U. K.

Vaughan, G., J. D. Price, and A. Howells (1994), Transport into the troposphere in a tropopause fold, *Q. J. R. Meteorol. Soc.*, *120*, 1085–1103.

Wakazuki, Y., K. Tsuboki, and T. Takeda (2006), Periodic evolution of multiscale precipitation systems developed within a Baiu frontal cloud cluster, *J. Meteorol. Soc. Jpn.*, *84*, 497–518.

Wei, M. Y. (1987), A new formulation of the exchange of mass and trace constituents between the stratosphere and troposphere, *J. Atmos. Sci.*, *44* (20), 3079–3086.

Yasunari, T., and T. Miwa (2006), Convective cloud systems over the Tibetan Plateau and their impact on meso-scale disturbances in the Meiyu/Baiu frontal zone—A case study in 1998, *J. Meteorol. Soc. Jpn.*, *84*, 783–803.

Yoshikane, T., F. Kimura, and S. Emori (2001), Numerical study on the Baiu front genesis by heating contrast between land and ocean, *J. Meteorol. Soc. Jpn.*, *79*, 671–686.

Zachariasse, M., P. F. J. van Velthoven, H. G. J. Smit, J. Lelieveld, T. K. Mandal, and H. Kelder (2000), Influence of stratosphere-troposphere exchange on tropospheric ozone over the tropical Indian Ocean during the winter monsoon, *J. Geophys. Res.*, *105*, 15,403–15,416.

Zhang, M., W. S. Tian, L. Chen, and D. R. Lü (2010), Cross-tropopause mass exchange associated with a tropopause fold event over the northeastern Tibetan Plateau, *Adv. Atmos. Sci.*, *27*(6), 1344–1360.

Zhou, Y. S., S. T. Gao, and S. S. P. Shen (2004), A diagnostic study of formation and structures of Meiyu front system over east Asia, *J. Meteorol. Soc. Jpn.*, *82*, 1565–1576.

Zhu, Q. G., J. R. Lin, S. W. Shou, and D. S. Tang (2007), Principles and Methods of Synoptic Meteorology [in Chinese], 351–354 pp., Meteorol. Press, Beijing.